Biomech Model Mechanobiol (2017) 16:667–679
DOI 10.1007/s10237-016-0844-8

ORIGINAL PAPER

Multiscale modeling of growth plate cartilage mechanobiology

Jie Gao[1] · **John L. Williams**[2] · **Esra Roan**[2]

Received: 23 February 2016 / Accepted: 12 October 2016 / Published online: 21 October 2016

Abstract Growth plate chondrocytes are responsible for bone growth through proliferation and differentiation. However, the way they experience physiological loads and regulate bone formation, especially during the later developmental phase in the mature growth plate, is still under active investigation. In this study, a previously developed multiscale finite element model of the growth plate is utilized to study the stress and strain distributions within the cartilage at the cellular level when rapidly compressed to 20 %. Detailed structures of the chondron are included in the model to examine the hypothesis that the same combination of mechanoregulatory signals shown to maintain cartilage or stimulate osteogenesis or fibrogenesis in the cartilage anlage or fracture callus also performs the same function at the cell level within the chondrons of growth plate cartilage. Our cell-level results are qualitatively and quantitatively in agreement with tissue-level theories when both hydrostatic cellular stress and strain are considered simultaneously in a mechanoregulatory phase diagram similar to that proposed at the tissue level by Claes and Heigele for fracture healing. Chondrocytes near the reserve/proliferative zone border are subjected to combinations of high compressive hydrostatic stresses (−0.4 MPa), and cell height and width strains of −12 to +9 % respectively, that maintain cartilage and keep chondrocytes from differentiating and provide conditions favorable for cell division, whereas chondrocytes closer to the hypertrophic/calcified zone undergo combinations of lower compressive hydrostatic stress (−0.18 MPa) and cell height and width strains as low as −4 to +4 %, respectively, that promote cell differentiation toward osteogenesis; cells near the outer periphery of the growth plate structure experience a combination of low compressive hydrostatic stress (0 to −0.15 MPa) and high maximum principal strain (20–29 %) that stimulate cell differentiation toward fibrocartilage or fibrous tissue.

Keywords Cartilage · Finite element model · Multiscale model · Chondron · Skeletal development · Physis

✉ John L. Williams
john.williams@memphis.edu

[1] Department of Mechanical Engineering, University of Memphis, Memphis, TN 38135, USA

[2] Department of Biomedical Engineering, University of Memphis, Memphis, TN 38135, USA

1 Introduction

Bone is formed by one of two basic processes: endochondral and intramembranous ossification. Endochondral bone formation is primarily involved in the long bone formation by replacing a hyaline cartilage 'model' or anlage by bone. In early development, the cartilage anlage grows along the long axis of what will become the long bone by continuous chondrocyte division and extracellular matrix secretion. The anlage also grows transverse to the long axis when cells from the perichondrium secrete extracellular matrix at the periphery of the long bone.

Around birth, in most mammals, a secondary center of ossification appears at both epiphyseal ends of a long bone. The bone then grows from the secondary ossification center in two directions: toward the joint and toward the primary ossification center in the diaphysis. The cartilage that is left between the primary and secondary ossification centers is called the epiphyseal plate (growth plate). The thickness of this plate is gradually reduced until a thin undulating layer shaped by mammillary processes remains. In humans, this thin layer (0.5–3 mm) continues to grow for many years to produce new cartilage, which is replaced by bone, thereby

increasing the length of the bone. While chemical factors, such as oxygen tension and many biological factors (Kronenberg 2003), regulate bone growth at this later stage of development (Mackie et al. 2008), there is abundant clinical and experimental evidence that mechanical factors also play a role in regulating bone growth (Frost 1990; Mao and Nah 2004; Villemure and Stokes 2009). However, among the various mechanoregulatory bone growth theories that have been proposed (Hueter 1863; Volkmann 1862; Pauwels 1960; Carter and Wong 1988b; Frost 1997; Stokes 2002), to our knowledge none have been shown to apply specifically at the microscale level to the thin layer of growth plate cartilage during the later stages of growth, which can last for many years.

Hueter (1863) and Volkmann (1862) observed clinically that greater than normal compression across the physis reduced normal growth whereas less than normal compression led to overgrowth. These observations are referred to in the current literature as the Hueter–Volkmann "law" or principle which is widely accepted as a concept of growth modulation. There is little in the way of experimental work to provide exact limits of stress or strain magnitude, time duration, frequency, strain or loading rate, number of cycles of loading, etc. In vivo loading experiments suggest a linear relationship exists between sustained static stress magnitudes and change in growth rate over the range of stresses examined (Stokes et al. 2006, 2007). By comparison, dynamic compressive loading has been suggested to be as efficient but more conservative than static loading for bone growth modulation (Valteau et al. 2011).

The predominant mechanoregulatory theories considered today are extensions of these ideas and those originally expressed by Pauwels (1960, 1965, 1980). Pauwels proposed that the differentiation pathway of mesenchymal cells is determined by two types of stress, either pure distortion of shape by stretch or pure change in volume by hydrostatic stress. Carter and colleagues further developed these ideas to include growth modulation aspects by proposing that the speed of endochondral ossification within the cartilage model is accelerated by cyclic octahedral shear stresses (which are accompanied by tensile principal stresses or strain) and slowed by cyclic compressive dilatational stresses (Carter et al. 1988; Carter and Wong 1988a; Wong and Carter 1990). These theories have coalesced around the hypothesis that octahedral shear stress (or tensile strain) promotes either ossification of cartilage or formation of fibrous tissues, while hydrostatic stress tends to maintain the cartilage.

The phase diagrams utilized during the evolution of these mechanoregulatory theories of Pauwels (1980) and Carter and coworkers (Carter et al. 1987; Carter and Wong 1988b, 1990; Carter and Orr 1992; Carter et al. 1998) were reformatted in a quantitative form by Claes and Heigele (1999) by comparing stresses and strains in a finite element (FE) model to the developing fracture callus histology at different stages of fracture healing. Since fracture repair or bone regeneration and endochondral ossification invoke a similar process of osteogenesis (Ferguson et al. 1999), similar mechanoregulatory theories have been proposed for both. Claes and Heigele (1999) showed that endochondral ossification was associated with compressive stresses larger than about -0.15 MPa and strains smaller than $+/-15$ %. Intramembranous bone formation coincided with strains smaller than approximately $+/-5$% and hydrostatic pressures smaller than $+/-0.15$ MPa. All other conditions seemed to lead to connective tissue or fibrous cartilage.

To explore the relevance of mechanoregulatory concepts at the chondron and chondrocyte level, we used a 3D multiscale FE model of the growth plate that we previously developed to investigate chondrocyte stress and strain distributions within the growth plate (Gao et al. 2015). Gao et al. (2015) presented the cell stress, strain and aspect ratio distributions as a function of location within the chondron and within a growth plate specimen and provided the details of the FE model and its assigned material properties. It examined the influence of the physeal free surface (at the periphery of the explant) on stresses and strains developed within chondrons near the free surface in comparison with those in the interior. In the present work, our model assumes an already established thin growth plate layer with chondrocytes arranged in columnar arrangement. It does not explain how this arrangement develops, which is an event occurring during the development of the secondary centers of ossification, preceding the mature stage of the growth plate that our model is concerned with. From the work of Claes and Heigele (1999) as summarized in their quantitative phase diagram in Fig. 1, one can infer that superimposed hydrostatic stresses and strains stimulate cells to go down one of several pathways, to form intramembranous bone, endochondral bone, fibrocartilage tissue or fibrous tissue.

We hypothesized that the same combination of macroscopic tissue-level mechanoregulatory signals (hydrostatic stress and maximum tensile strain) shown to maintain cartilage or stimulate osteogenesis or fibrogenesis in the cartilage anlage or fracture callus also performs the same function at the cell level within the organization of chondrons in growth plate cartilage. Our objective was to determine whether moderate compressive loading of the growth plate produces a gradation in the combination of cellular compressive hydrostatic stresses and maximum tensile strains from the proliferative down to the hypertrophic zone that is consistent with the known cellular function in these zones. We refer to the combination of absolute values of hydrostatic stress and maximum strain as the mechanoregulatory state function (MSF), a function that is closely related to the osteogenic index, which is a combination of cyclic octahedral shear and hydrostatic stress proposed for endochondral ossification proposed by Carter and Wong (1988a, b).

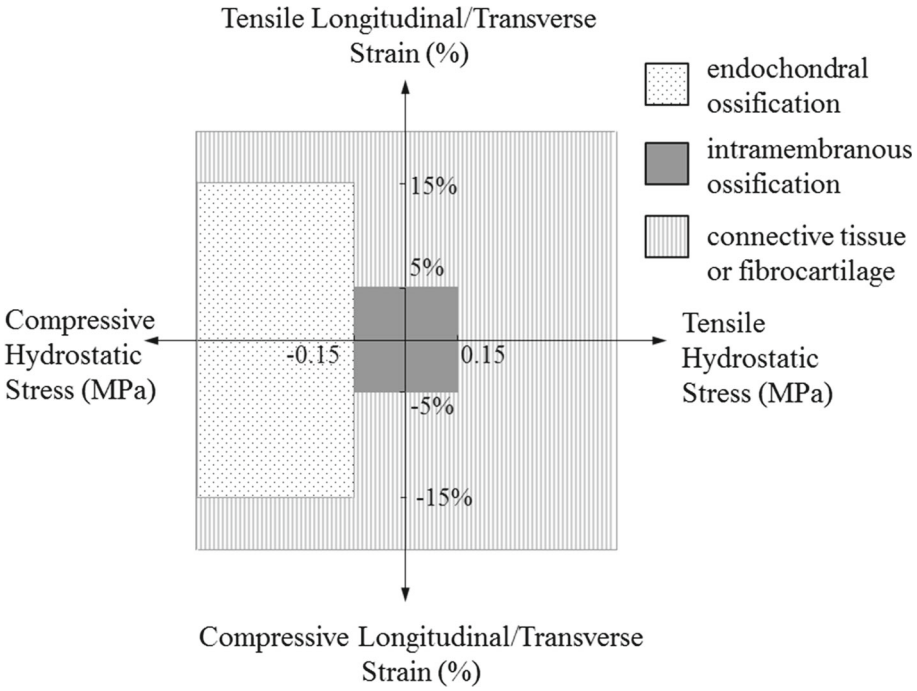

Fig. 1 Schematic of tissue differentiation (mechanoregulatory) phase diagram used for modeling bone fracture healing (adapted from Claes and Heigele (1999))

Specifically, we asked whether (1) the MSF in chondrocytes in the proliferative zone produces conditions that maintain cartilage, prevent cell differentiation and perhaps favor cell division (large MSF); and (2) the MSF decreases along the chondron through the zone of maturation and reaches a minimum value in the hypertrophic zone, conditions that favor differentiation and osteogenesis.

2 Methods

2.1 Model description

A multiscale large displacement static FE submodeling approach was utilized in this study with ABAQUS version 6.12 (Simulia, Providence, RI) in order to determine how the macroscopic loads are transmitted through the microstructure of the growth plate to the chondrocytes. The model has been described in detail elsewhere (Gao et al. 2015). Two simplified shapes (flat and 'm' shapes) of the growth plate were modeled in order to examine the influence of mammillary processes on stresses and strains (Fig. 2a). Limiting geometric variation in one direction of the growth plate while allowing it in the other allows the influence of geometry to be explored in 3D. Moreover, some growth plates of this size show minor variation in shape along one of the directions parallel to the physis as indicated in our idealized model (see, for example, the distal rabbit femoral physis in Lerner et al. 1998). Multiscale submodeling was used to study the transmission of loads from the macroscopic structure (in millimeters) to microscopic structures such as cells (in microns) (Fig. 2b). A $7 \times 7 \times 7$ mm model of a bone-growth plate-bone sample was constrained in all directions at the base ($Y = 0$), and a compressive displacement equal to 20 % of the growth plate thickness was applied at the top surface along the long (Y) axis of the bone, resulting in an average vertical reaction pressure of 0.4 MPa at the fixed surface. Ten equal incremental steps were used to reach the final displacement. Isotropic linear elastic materials were used in a large displacement analysis to simulate the response of instantaneous loading applied on top of the model. The elastic modulus of interterritorial matrix (ITM) gradually changed from 0.38 to 1.87 MPa (Radhakrishnan et al. 2004) (Fig. 3), while the elastic modulus of the territorial matrix (TM) and chondrocytes was taken to be 0.26 MPa (Allen and Mao 2004) and 2 kPa (Leipzig and Athanasiou 2005; Ng et al. 2007), respectively (Gao et al. 2015). Chondrocytes were assumed to be incompressible (Poisson's ratio = 0.5). Fluid effects were ignored due to the assumption of short-time-scale loading. Mesh convergence studies were performed at each scale to ensure adequate mesh sizes for the models used in the study.

The macroscale model consisted of 181,056 eight-node hexagonal elements with reduced integration (C3D8R). Mesoscale models (three-layered and ten-layered model) consisted of 159,848 and 119,700 eight-node hexagonal elements with reduced integration (C3D8RH), respectively. As for the microscale level, the chondron model consisted of 268,455 hybrid four-node tetrahedral (C3D4H) elements for cells and general purpose four-node tetrahedral C3D4 elements with reduced integration for the TM and ITM. Reduced integration formulation was used to prevent volumetric locking and save computational time. Hybrid elements

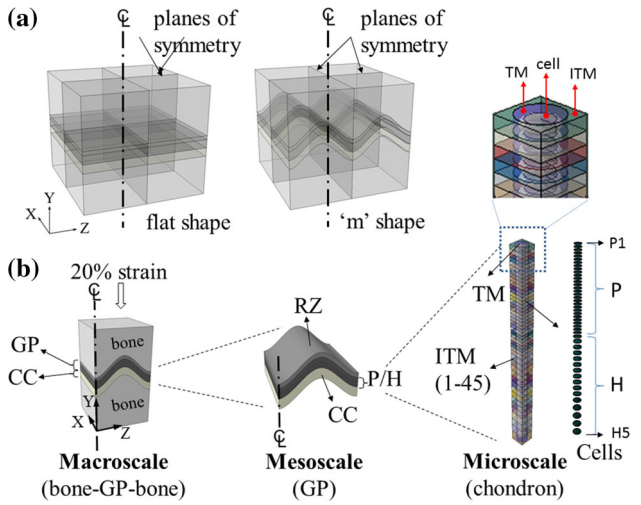

Fig. 2 **(a)** Two idealized models were constructed consisting of epiphyseal bone, growth plate (GP) cartilage and metaphyseal bone (about $7 \times 7 \times 7$ mm) with variations of mammillary processes: flat and '*m*' shaped. **(b)** Schematic of the multiscale modeling approach. At the macroscale level, quarter models were used for analysis. Growth plate cartilage (0.69 mm in height) was partitioned into two sections to represent the reserve zone (RZ) and the proliferative/hypertrophic (P/H) zone. Calcified cartilage (CC) was also included in the macroscale model. A compressive displacement equal to 20 % of the growth plate height was prescribed at the top surface in the direction along the long axis of the bone. At the mesoscale level, three individual layers were generated in the P/H zone to represent the gradient change in elastic modulus through the thickness of the growth plate. The microscale model of the chondron consisted of interterritorial matrix (ITM), territorial matrix (TM) and 46 chondrocytes with gradually changing cellular shape along with the same number of ITM sections. The elastic modulus of ITM increased from the RZ to the metaphyseal side to represent the gradual change in its material properties. As a model simplification the chondrocyte widths remained unchanged along the length of the chondrons whereas these normally increase as shown in Fig. 3

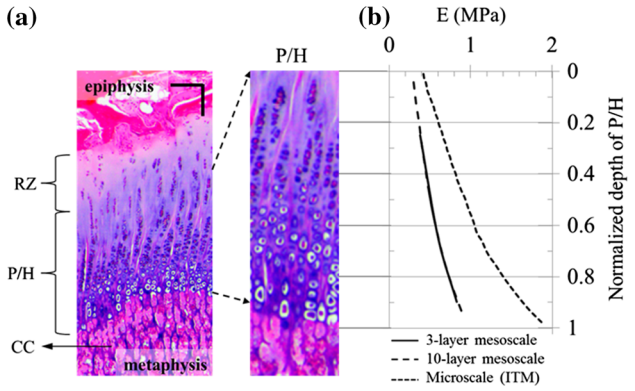

Fig. 3 Determination of the elastic moduli of the growth plate utilized in the models. **a** Stained histological slice (hematoxylin and eosin) of a 4-month-old bovine growth plate; chondrocytes are dispersed in the reserve zone (RZ) and are stacked in tubes (chondrons) extending from the zone of proliferation (P) through the zones of maturation and hypertrophy (H). The walls of the chondron tubes (interterritorial matrix) become increasingly calcified toward the metaphyseal side. Following chondrocyte death, the walls of tubes or bars of calcified cartilage (CC) matrix form the scaffolding upon which bone is laid down (primary spongiosa); scale bar = 100 μm. **b** Distribution of the elastic modulus of the P/H zone (three-layered mesoscale and ten-layered mesoscale models) and interterritorial matrix (ITM) (microscale model) (from: Gao et al. 2015)

with enhanced hourglass control (C3D8RH for macroscale and mesoscale models, C3D4H for microscale model) were utilized for incompressible materials to remedy potential locking problems during the analyses. Further details of the model are provided elsewhere (Gao et al. 2015).

2.2 Averaged cell stress and strain calculation

The average hydrostatic stress (σ_i) in each chondrocyte was calculated as:

$$\text{Average cellular stress} = \sum_{i=1}^{n} \sigma_i \text{Evol}_i \Big/ \sum_{i=1}^{n} \text{Evol}_i, \tag{1}$$

where i is the ith element within the same chondrocyte which includes a total number of n elements, σ_i is the stress at the integration point of each element and *Evol* is the element volume. Compressive hydrostatic stress is negative.

The average maximum principal strain (ε_i) in each chondrocyte was calculated:

$$\text{Average cellular strain} = \sum_{i=1}^{n} \varepsilon_i \big/ n, \tag{2}$$

where i is the ith element within the same chondrocyte which includes a total number of n elements, ε_i is the strain at the integration point of each element. Maximum principal strain is tensile strain and is positive.

2.3 Strain measures

All strain results were directly extracted from the analysis as logarithmic strains (LE) with the exception of cell height and width strains. Chondrocyte height and width strains were reported as engineering strain from the measurements of the cell heights and widths. The cell-averaged maximum principal strains and the cell-averaged hydrostatic stresses were used to create a tissue differentiation phase diagram similar to that proposed by Claes and Heigele (1999). The vertical axis in their phase diagram corresponds to strains (positive or negative) parallel and transverse to the bone long axes, or in a coordinate system with axes aligned along and transverse to the ossification front, when comparing the model of fracture healing to the experimental observations. Similarly, our chondrocyte width and height strains in the chondrons are aligned along and transverse to the bone long axis.

We also calculated maximum (tensile) principal strain to replace cell height and width strain for comparison purposes although there are no quantitative studies to evaluate these magnitudes in association with proliferation and differentiation. We believe that principal strains are of interest because they develop in different directions and may be related to what cells sense in their environment within the chondron and through connection to the pericellular or territorial matrix (TM), and also because principal tensile strain was used for the y-axis in the phase diagrams in the later publications of Carter et al. (1998). Although we used a single-phase material model, the hydrostatic stress would be expected to be borne by the fluid phase and the principal tensile strain by the fibrous component of the solid phase. The fibrous or tension-bearing components, although not represented as such in the model, are oriented in directions different from the major and minor axes of the cell which are used to determine cell height strain and width strain.

3 Results

Stresses and strains (absolute values) decreased within the chondron from the base of the proliferative zone, adjacent to the reserve zone, toward the last cell in the hypertrophic zone. Near the center line ($X = 0$, $Z = 0$) of the model, the proliferative chondrocytes experienced greater hydrostatic stresses (absolute value) and greater maximum principal strains (logarithmic strain, LE) than hypertrophic chondrocytes (Fig. 4). The results were calculated for a chondron slightly off center for the '*m*'-shaped growth plate. The peak values for hydrostatic compressive stress (−0.38 MPa) and maximum principal (tensile) strain (12 %) gradually decreased from the proliferative zone down to −0.17 MPa and 7 %, respectively at the calcified cartilage border of the chondron. Results extracted from the flat-shaped growth plate (not shown) were found to follow similar trends as for the '*m*'-shaped growth plate. By comparison, the average tissue level strains for a model without chondrons and cells were 15 % across the reserve through hypertrophic zones.

Chondrocyte hydrostatic stresses within each zone remained relatively constant in the direction transverse to the bone long axis, except near the outer surface where the proliferative and hypertrophic chondrocyte hydrostatic stresses dropped to −0.14 and −0.04 MPa, respectively (Fig. 5). Proliferative chondrocytes experienced higher hydrostatic stress (absolute value) than hypertrophic chondrocytes at each location from the center toward the edge. The gradient in hydrostatic stress from the proliferative to the hypertrophic zone remained relatively constant until the outer edge where the gradient decreased to less than half the gradient in the central region. Similar trends were observed for the flat-shaped growth plate model, although the flat-shaped growth plate

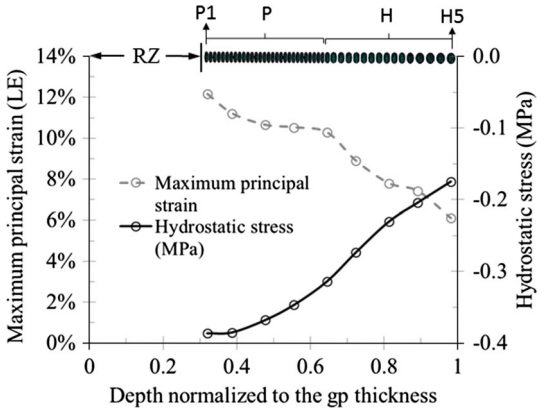

Fig. 4 Distributions of maximum principal strain (logarithmic strain, LE) and hydrostatic stress obtained from the microscale model within the '*m*'-shaped growth plate subjected to 20 % compression (15 % across the reserve zone through hypertrophic zones). Stresses were averaged for each chondrocyte embedded in a chondron. The results were obtained for a (30 μ wide) chondron centered at $X = 0$, $Z = 75$ μ near the central region of the growth plate. Proliferative chondrocytes experienced higher hydrostatic stress (absolute value) than hypertrophic chondrocytes. Cell stresses for a flat-shaped growth plate followed a similar trend as for the '*m*'-shaped growth plate model. In both the flat- and '*m*'-shaped models, the cellular tensile strains decreased from the proliferative to hypertrophic zones

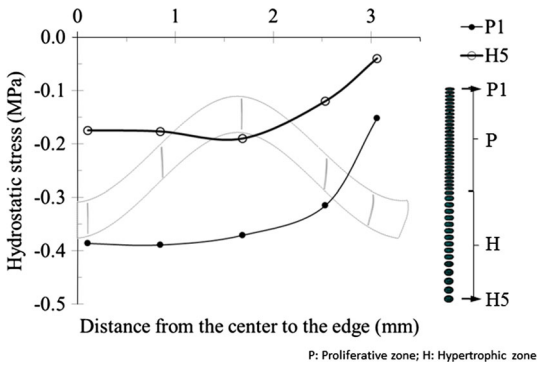

Fig. 5 Distribution of the cell-averaged hydrostatic stress obtained from the microscale model with chondrocytes embedded in a chondron within the '*m*'-shaped growth plate (shown in *gray*) subjected to 20 % compression (15 % across the reserve zone (RZ) through hypertrophic zones). The results were extracted from five different locations in the plane transverse to the bone long axis. Chondrocytes at all zonal levels experienced higher hydrostatic stress (absolute value) in the central region than in the region close to the outer surface. Proliferative (P) chondrocytes experienced higher hydrostatic stress (absolute value) than hypertrophic (H) chondrocytes

experienced relatively greater (about 10 %) hydrostatic stress (absolute value) than the '*m*'-shaped growth plate at the cell level (results not shown).

Chondrocyte maximum (tensile) principal logarithmic strains (LE) varied with location along the direction transverse to the bone long axis and in relation to the mammillary process. Proliferative chondrocytes located on the sloped regions of the 'm'-shaped mammillary processes experi-

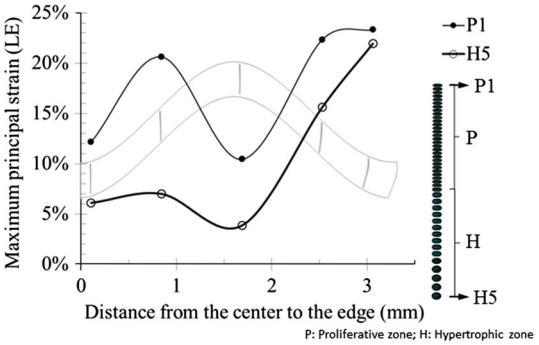

Fig. 6 Distribution of maximum principal logarithmic strains (LE) obtained from the microscale model with embedded chondrocytes within the 'm'-shaped growth plate subjected to 20 % compression (15 % across the reserve zone through proliferative (P) and hypertrophic (H) zones). The results were extracted from five different radial locations from the center to the edge of the growth plate. Chondrocytes located at the sloped regions of the 'm'-shaped growth plate experienced higher maximum principal strain (LE) than those located at other regions (except for the region close to the outer edge) regardless of the zonal location of the chondrocytes

enced higher maximum principal strains (LE = 21–23 %) compared with those located near the central valley and apex of the mammillary processes (LE = 10–12 %), except for the region close to the outer edge, where the strains were largest (LE = 24 %). Cells in the hypertrophic zone varied similarly, except on the interior slope of the mammillary processes (Fig. 6). Proliferative chondrocytes experienced greater maximum principal strains than hypertrophic chondrocytes at every location in the transverse plane. The gradient in principal strain from the proliferative to the hypertrophic was greatest on the interior slope of the mammillary processes and smallest at the periphery. Regarding the flat-shaped growth plate model, similar trends were observed with slightly lower maximum principal strain compared with the '*m*'-shaped growth plate at the cell level (results not shown).

Chondrocyte height and width strains versus cell-averaged hydrostatic stresses are shown in a phase diagram for chondrocytes in the central region of the growth plate in Fig. 7. Chondrocytes located within the interior of the growth plate had strain and stress values that remain close to or within the quantitative bounds determined to be necessary for osteogenesis in a fracture healing callus (Claes and Heigele 1999). Chondrocytes near the reserve/proliferative zone border were subjected to combinations of high compressive hydrostatic stresses (−0.4 MPa), and cell height and width strains of −12 to +9 %, respectively, that maintain cartilage and keep chondrocytes from differentiating, whereas chondrocytes closer to the hypertrophic/calcified zone were exposed to lower compressive hydrostatic stresses (−0.18 MPa) and to cell height and width strains as low as −4 % to +4 %, respectively, that promote cell differentiation toward osteogenesis.

The chondrocyte maximum principal strain (LE) values were slightly greater in magnitude compared with cell height and width strain as would be expected (Fig. 8). The maximum principal strain gradient in the phase diagram was steeper as strains dropped along the chondron from a peak of 12–21 % in the first proliferative or daughter cell (where the hydrostatic stress is −0.39 MPa) down to 7 % in the last hypertrophic chondrocyte (where the hydrostatic stress has decreased to −0.18 MPa). Hydrostatic pressures and principal tensile strains in terminal chondrocytes at the border of the calcified zone approached limits determined in fracture healing for intramembranous ossification (Fig. 8). Cells near the outer periphery of the growth plate structure experienced a combination of low compressive hydrostatic stress (0 to −0.15 MPa) and high maximum principal strain (LE = 20–29 %) that would be expected to stimulate cell differentiation toward fibrocartilage or fibrous tissue (Claes and Heigele 1999).

Hydrostatic stresses and maximum principal strains (LE) were plotted for the microscale model in the central region of the '*m*'-shaped growth plate model to show interactions between chondrocytes and their surrounding matrix (Fig. 9). Border regions of the chondrocytes adjacent to territorial matrix (TM) exhibited slightly higher strains than the interior regions of the chondrocytes. All chondrocytes, TM and ITM were exposed to higher pressure in the proliferative zone than in the hypertrophic zone. At each zonal location, chondrocytes were subjected to higher hydrostatic stress than their surrounding matrix (TM) (Fig. 9a). In addition, chondrocytes experienced higher maximum principal strain (LE) than their surrounding TM. Within each chondrocyte, the cell/matrix boundary experienced higher strain levels than the central region of the cell (Fig. 9b, c). In the proliferative zone, the ITM was compressed (Fig. 9c upper), whereas in the hypertrophic zone, the TM was compressed (Fig. 9c lower). The hypertrophic ITM was subjected to more tensile strain than proliferative the ITM, while proliferative chondrocytes also experienced more tensile strain than hypertrophic chondrocytes (Fig. 9d).

4 Discussion

The results indicate that (1) the MSF in chondrocytes in the proliferative zone produces conditions that maintain cartilage (Fig. 4), prevent cell differentiation and perhaps favor cell division (large MSF); and (2) the MSF decreases along the length of the chondron from the proliferative through the zone of maturation and reaches a minimum value in the hypertrophic zone, conditions that favor differentiation and osteogenesis, as was hypothesized. Therefore, the model supports the hypothesis that the same mechanoregulatory signals found to regulate fracture healing at the tissue level also

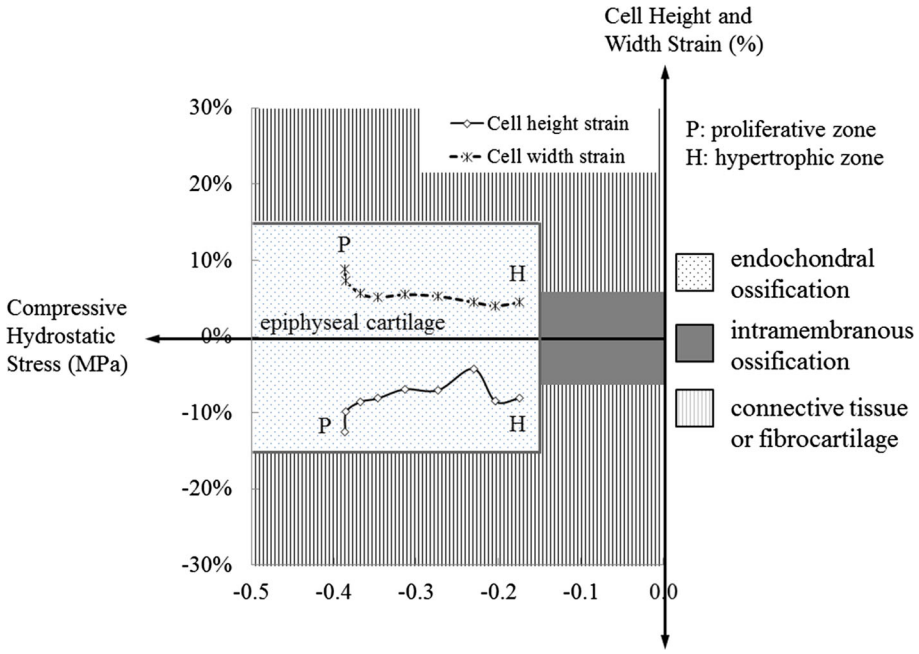

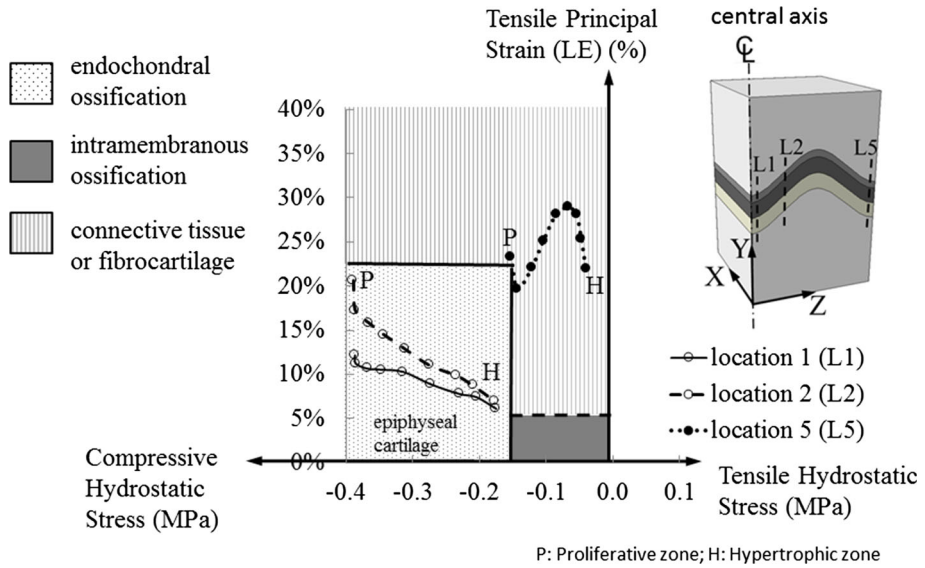

Fig. 7 Chondrocyte height and width strains for the central chondron of the '*m*'-shaped growth plate subjected to 20 % compression across the growth plate (15 % across the reserve through hypertrophic zones) are shown to fall within the strain ($+/-15\,\%$) and stress (> 0.15 MPa in compression) limits established for by Claes and Heigele for endochondral bone formation in fracture healing (Claes and Heigele 1999). The results were obtained for a (30 μm wide) chondron centered at $X = 0$, $Z = 75\mu$m near the central region of the growth plate

Fig. 8 Cell-averaged hydrostatic stress and maximum principal (tensile) strain from Figs. 4 and 5 plotted on a schematic similar to that proposed for fracture healing (Claes and Heigele 1999) except that strains are shown as maximum (tensile) principal strains (LE) rather than as strains along and perpendicular to the growth front. For locations within the central region of the growth plate model (positions 1 and 2), the proliferative chondrocytes (P) closest to the reserve zone experienced cell-averaged maximum tensile strains slightly greater than the $+/-15\,\%$ the tissue-level strain limits established for endochondral bone formation in fracture healing for tissue level strains in the direction of the growth front or perpendicular to it. For most of the central region of the growth plate, the terminal hypertrophic chondrocytes (H) bordering the calcified cartilage zone approach the stress and strain limits determined by Claes and Heigele for membrane bone formation; chondrons located within 1 mm of the periphery (position 5) fall within the fibrous tissue and fibrocartilage regions established for fracture healing

function at the chondrocyte level in the physis to control longitudinal bone growth. The phase diagram in Fig. 7 indicates that for a strain of 20 % applied across the growth plate the compressive hydrostatic stresses (-0.15 to -0.4 MPa), cell width (-3 to $-10\,\%$) and height strain ($+4$ to $+13.5\,\%$) magnitudes in a centrally located chondron of the epiphyseal cartilage fall within the bounds determined at the tissue level for endochondral bone formation in fracture healing (Fig.1) by Claes and Heigele (1999). The phase diagram for maximum principal strains and hydrostatic stresses in growth plate chondrocytes in relation to their known cell function (maintenance of cartilage versus differentiation toward osteogenesis)

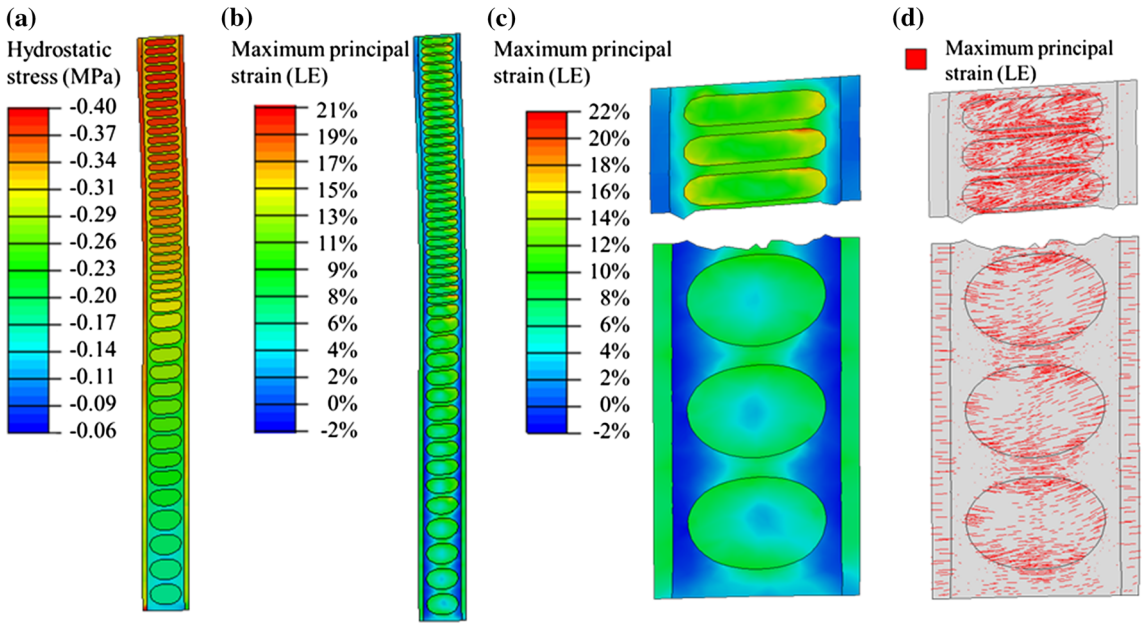

Fig. 9 Distributions of hydrostatic stress and maximum principal logarithmic strain (LE) within the microscale model near the central region of the '*m*'-shaped growth plate model. Contour changes are shown when the results in adjacent elements differ by more than 25 %. **a** Pressure distribution within the microscale model. Chondrocytes, TM and ITM all experienced higher pressure at the proliferative zone than the hypertrophic zone. At each zonal location, chondrocytes experienced higher pressure than their surrounding matrix (TM). **b, c** Maximum principal strain (LE) distribution within the microscale model. Chondrocytes experienced higher strain than surrounding TM. Within each chondrocyte, the border region of cell and matrix experienced higher strain than the central region of the cell. At the proliferative zone (**c**), ITM experienced compressive maximum principal strain. This is due in part to the lateral expansion of incompressible cells pushing against the ITM, so that the ITM was being compressed at this region. However, at the hypertrophic zone (**c**), it is the TM that being compressed. This is probably because the elastic modulus of the hypertrophic ITM is higher than the proliferative ITM, while the elastic modulus of TM is constant. Therefore, when cells in the proliferative zone are being compressed to expand laterally, the TM provides the buffer zone instead of ITM. **d** Directions of maximum principal strain (LE) within the upper proliferative and lower hypertrophic zones (3D vectors are transected in the viewing plane)

is qualitatively similar to that for tissue level studies of fracture healing. Our findings are for one particular loading case (fast compression to 20 %) and our results are discussed in relation to this one particular loading case only, but are likely relevant to the cellular level mechanoregulatory processes in the physis.

The results indicate that there is a correlation between hydrostatic stress at the cellular level in the thin layer of growth plate cartilage and the chondrocyte morphology and function in the various zones of the growth plate as chondrocytes progress through the stages of proliferation and hypertrophy and terminal differentiation. Chondrocytes located close to the metaphysis experienced less hydrostatic stress than those close to the reserve zone, and these regions correspond with the location of cartilage calcification during the bone development. In cell culture studies, cyclic (0.5 Hz) hydrostatic pressure has been shown to down regulate the expression of MMP-13 (matrix metallopeptidase 13, the main proteolytic enzyme in hypertrophic cartilage (Vinardell et al. 2012) and type I collagen in articular cartilage chondrocytes (Wong et al. 2003). Another study suggested that hydrostatic stress may reduce the rate of chondrocyte differentiation and have an anti-angiogenic influence on cartilage (Wong et al. 2003) and inhibit endochondral ossification (Lerner and Kuhn 1997). Based on information from these previous studies (Carter et al. 1988; Wong et al. 2003; Vinardell et al. 2012), hypertrophic chondrocytes would be expected to experience lower hydrostatic stress than proliferative chondrocytes, which agrees with our results. On the other hand, chondrocytes located close to the periphery of the growth plate experienced less hydrostatic stress and these regions correlate with the location of faster bone growth during the bone development (Lerner and Kuhn 1997).

Therefore, (1) the MSF in chondrocytes in the proliferative zone produces conditions that maintain cartilage, prevent cell differentiation (large MSF) and perhaps provide conditions favorable to cell division; and (2) the MSF decreases along the chondron through the zone of maturation and reaches a minimum value in the hypertrophic zone, conditions that favor differentiation and osteogenesis (Fig. 4). It has been shown in 2D cultures that chondrocytes subjected to cyclic tensile strains of 3–17 % at frequencies greater than

0.17 Hz stimulate chondrocytes to divide (Bleuel et al. 2015). Although extrapolation from 2D cell culture to 3D organ levels is simplistic, it may be that the maximum tensile strains seen to develop primarily in the transverse (lateral direction) of the physis (Fig. 9d) provide a favorable environment for chondrocyte division, which occurs in the transverse direction after which the daughter cell reorients itself vertically beneath the mother cell.

Our cell-averaged strain results, when considered on their own, seem to contradict the mechanobiological theories. The relevance of mechanoregulatory theory at the cellular level only becomes clear when strains are considered in combination with hydrostatic stresses in a mechanoregulatory phase diagram. Based on the theory that exposing chondrocytes to shear stress (or maximum principal strain) drives the synthesis of those proteins which are responsible for angiogenesis and later acceleration of cartilage ossification (Carter and Wong 2003), it would be reasonable to expect higher octahedral shear stress (or maximum principal strain) in the hypertrophic chondrocytes than in the proliferative zone. Experiments have shown that cyclic (0.5 Hz) tension appears to activate the Cbfa1/MMP-13 pathway and increase the expression of terminal differentiation hypertrophic markers (such as type X collagen) in articular chondrocytes (Wong et al. 2003). However, when both cell-averaged hydrostatic stress and maximum principal strain are considered simultaneously (for cells in a chondron located in the interior) and plotted on the phase diagram, the predicted differentiation gradient of chondrocytes within the chondron is qualitatively consistent with the mechanoregulatory concepts proposed for early endochondral bone formation (Carter and Wong 1988b; Carter et al. 1998; Loboa et al. 2003) and in quantitative agreement with the mechanoregulatory phase diagram proposed for fracture healing (Claes and Heigele 1999).

The model results are also consistent with the mechanoregulatory ideas that large tensile strains promote fibrous tissue and fibrocartilage formation when the chondron is located near the outer periphery of the growth plate where in an actual bone the hyaline cartilage merges into a fibrous or fibrocartilaginous perichondrium (Fig. 8). Figure 8 also shows the principal strain values superimposed with hydrostatic stresses for cells near the perichondrial border of the growth plate. In life, a slight circumferential indentation is formed at the surface of the bone where the growth plate is located, which was originally described by Ranvier and subsequently referred to as the node of Ranvier or Ranvier's groove. This region contains undifferentiated mesenchymal cells responsible for the increase in width of the epiphysis. Some of these cells pass through the developmental stages from germinal to proliferation to hypertrophic cells, thereby increasing the transverse diameter of the physis (Shapiro et al. 1977; Solomon 1966; Hert 1976). Also present in the groove of many physes is a thin tube of intramembranous bone (called bone bark) encircling the lower portion of the growth plate, which in our opinion would restrain the most peripheral chondrons from buckling outward. Additionally, fibroblasts are present within sheets of highly oriented collagen fibers that are continuous with the outer fibrous layer of the perichondrium and periosteum and with the epiphyseal cartilage (Shapiro et al. 1977). This complex structure is omitted from our model, and its possible influence on the stresses and strains in the most peripheral chondron is absent from our model results.

In our model, the values for maximum principal strain in chondrocytes at the periphery are 4–5 times larger than the limits ($+/-5\,\%$) for intramembranous bone formation shown in the phase diagram of Claes and Heigele, suggesting that this would fall within the region of fibrous tissue in Claes and Heigele's quantitative phase diagram, rather than region of intramembranous bone formation. However, our model does not contain any representation of Ranvier's groove, and it is conceivable that at the stage of development for which our model is applicable the bone bark tube (if present) would restrain the most peripheral chondrons and therefore alter the state of stress and strain in the most peripheral chondrons. The values we have noted in our phase diagram using maximum principal strains for intramembranous bone formation at the perichondrial border in the node of Ranvier would need to be explored experimentally, and the model would need to include a representation of the relevant tissues and cells in Ranvier's groove. We therefore consider the hydrostatic stress and maximum principal strain boundaries plotted for the results in this peripheral region on our phase diagram as hypothetical.

When cellular strains are characterized in terms of chondrocyte height and width and plotted on a mechanoregulatory type of diagram (Fig. 7) along with their cell-averaged hydrostatic stresses, it can be seen that the entire growth plate is exposed to conditions favorable for endochondral bone formation according to the strain and stress limits determined for endochondral bone formation in the fracture callus (Claes and Heigele 1999). Without in vivo experiments, our study is not capable of providing suggestions on potential limits beyond which either injury or growth arrest might occur. Based on our results, the strain limits appear to be reasonable starting point for further exploration. This view does not distinguish tension from compression, but requires the simultaneous consideration of deformation and hydrostatic stress, which is consistent with the early ideas of Pauwels regarding cell deformation when embedded in a tissue being deformed under uniaxial loading.

One way chondrocytes are known to sense mechanical signals from their surrounding matrix is through the stretching of their plasma membrane (Sachs 1991; Watson 1991; Amini et al. 2010). In addition, primary cilia, which are antenna-like structures extruding from the surface of the cells, have

been found to sense fluid shear (Temiyasathit and Jacobs 2010; Winyard and Jenkins 2011) and have been reported to play an important role in bone development (Haycraft and Serra 2008; Seeger-Nukpezah and Golemis 2012; Shao et al. 2012). It is postulated that they sense mechanical loads that acting on the cells and transduce them into biological signals (Shao et al. 2012). In the growth plate, cilia bind to collagen fibers through ciliary integrin receptors (Jensen et al. 2004; Farnum and Wilsman 2011) and respond to mechanical signals from ECM (Seeger-Nukpezah and Golemis 2012). Our results show that the TM experienced different hydrostatic stress and tensile strain compared to chondrocytes from the same location. Considering these results together with the location and function of the primary cilia, it is reasonable to speculate that the primary cilia present one avenue for the growth plate chondrocytes to sense and transduce surrounding mechanical signals, even though no cilia were modeled in this study. Chondrocyte strains in our model are greatest at the border between the cell and the matrix rather than in the center (Fig. 9), which would support a possible role for ciliary mechanotransduction.

To the best of our knowledge, no experimental data have been published on chondrocytes within growth plate cartilage under instantaneous compression for us to compare our results to. Therefore, results obtained from articular chondrocytes from previous studies were used to make limited comparisons. One previous study (Chahine et al. 2007) surmised the internal pressure values of articular chondrocytes to be around 23 kPa under 2 % compressive strain during transient loading from their FE model of their experiment. Our results of pressures in chondrocytes extracted at the same strain level (2 %) were about 15–33 kPa (proliferative–hypertrophic) in the central region of the '*m*'-shaped growth plate model, which agree with this previous study (Chahine et al. 2007). The nominal stress within the macroscale model was calculated to be 0.4 MPa, which falls within the estimated physiologic range of joint loading during activities such as walking (Katta et al. 2009; Hosseini et al. 2010).

The current model is limited to fast loading (e.g., heal strike in walking) where the fluid component has no time to flow through the tissue. During gait the joints of the lower limb are subjected to cyclic loading. These loads are applied at fast rates and act for short durations (Mann and Hagy 1980). There is convincing experimental and theoretical evidence for using a single-phase linear elastic model for short duration loading of articular cartilage (Carter and Beaupré 1999; Higginson et al. 1976; Armstrong et al. 1984; Brown and Singerman 1986; Ateshian et al. 1994). Cartilage may be modeled as biphasic, viscoelastic or poroelastic when the relaxation time and the period of observation are of the same order of magnitude. Ignoring the fluid-dependent behavior is reasonable for transient loading such as impact during heel strike or during the 0.2-s segment of the stance phase of a gait cycle. The relaxation time for growth plate cartilage in our experiments at 20 % compression is around 1200 s (Tutorino et al. 2001), similar to values reported by Wosu et al. (2012), and chondrocytes have a relaxation time of 10–20 s (Darling et al. 2008; Appelman et al. 2011). Since cartilage permeability is low, fluid flow and nonlinear changes in stress and strain take place over a period of many minutes to hours, much longer than loading rates experienced during walking and running. We believe that our assumptions of linear elasticity are reasonable for the current application since it has been shown to phenomenologically simulate a wide variety of normal and abnormal bone growth scenarios. In relation to the objectives of the current work, Carter and Wong (2003) stated that "…similar analyses using poroelastic constitutive models have failed to provide any additional insights or change the basic conclusions drawn from the linear elastic models." However, it should be noted that while the chondrocyte volume remains nearly constant during instantaneous loading conditions the instantaneous bulk strains will be smaller compared to the equilibrium state.

In general, the assumption of linearity in the elastic material properties is reasonable for the purpose of describing the basic mechanical behavior of the growth plate under uniaxial compression and has been used in previous studies (Carter and Wong 2003; Piszczatowski 2011). Since we observed approximately linear stress–strain behavior up to 20 % strain in the experimental growth plate compression tests (Tutorino et al. 2001; Gao et al. 2014) used to develop our model (Gao et al. (2015)), we feel that the assumption of stress–strain linearity is reasonable up to 20 % strain. Similar approximate linear behavior is shown in compression tests of growth plate samples from the distal ulna of pigs eight weeks and older (Wosu et al. 2012).

We believe that 20 % is a physiological peak level of strain. Taking articular cartilage for comparison, it has been shown using an MRI-based method that maximum principal strains reach values of +10 and −10 % in the tibial and femoral articular cartilage of volunteers during compressive loading by cyclically applying one-half body weight at the foot, suggesting that at full body weight the dynamic tissue level principal strains would reach +20 and −20 % strain. (Chan et al. 2016), thereby providing similar strain levels to those applied to our model of growth plate cartilage. Our quantitative results are specific to the magnitude of the applied 20 % strain across the growth plate cartilage at a nominal stress of 0.4 MPa. Peak intermittent joint loads at the knee during walking are 3 x BW and during jogging 5 × BW. (Bergmann et al. 2014). Assuming a growth plate area at the proximal tibia in a 450 N adolescent of around 2, 800 mm^2, the average peak stress in the growth plate cartilage, if evenly distributed, would be 0.16 MPa standing on one leg, 0.48 MPa walking and 0.8 MPa jogging. For comparison, the peak compressive stresses acting along the bone axial direction in the

growth plate of the rabbit distal femur in the sitting position have been estimated to range from about 0.25 to 0.6 MPa in growing rabbits (Lerner et al. 1998). Hopping would presumably increase these stresses. These estimates are for intermittent peak stresses applied over short time intervals. It has been estimated that a sustained compressive stress of 0.6 MPa would result in a 100 % reduction in growth rate (Villemure and Stokes 2009). The magnitude of sustained compressive stress needed to cause growth arrest has been estimated at 0.3 MPa (Bonnel et al. 1983), 0.5 MPa (Safran et al. 1992) and 0.5–1 MPa (Bylski-Austrow et al. 2001).

Limitations of this study include the assumption that chondrocytes are continuously attached to the surrounding matrix as in other previous studies (Guilak and Mow 2000; Lai et al. 2013), even though these attachments are known to be discrete (Burridge et al. 1988). The topographies of the growth plate layer were simplified to represent idealized shapes observed in experimental samples of bovine growth plate (Tutorino et al. 2001). Furthermore, some structures (e.g., perichondrium, groove of Ranvier and ring of LaCroix) were not included. Potential structural support from these structures was not considered in this study, and this may lead to an overestimation of the lateral expansion at the growth plate outer perimeter. Our focus in this paper was on the biologically active structural and functional unit of the growth plate which is represented by the chondron. We did not develop a microscale model at the level of the cell for the reserve zone, which we plan to do in future.

In summary, the major limitations of the model include: linear elastic material properties representation of a single loading state representing 20 % compression at a fast loading rate corresponding to heal strike, idealized mammillary process geometry, simplified cell shapes, omission of fluid flow, cells within the reserve zone, the perichondrial structures and internal cellular detail (nucleus, cytoskeletal structures, etc.) and attachment structures between the cells and surrounding matrix (cilia, integrin, etc.).

5 Conclusions

In conclusion, this study utilized a multiscale FE model of growth plate cartilage under moderate instantaneous compression to test the hypothesis that the same combination of mechanoregulatory signals shown to maintain cartilage or stimulate osteogenesis or fibrogenesis in the cartilage anlage or fracture callus at the tissue level also performs the same function at the cell level within the chondrons of growth plate cartilage. To our knowledge, this study is the first attempt to compare qualitative or quantitative values for mechanoregulatory parameters at the individual cell level within the growth plate chondron. The model provides evidence to support the hypothesis. Our cell-level results are qualitatively and quantitatively in agreement with tissue-level theories when both hydrostatic cellular stress and strain are considered simultaneously in a mechanoregulatory phase diagram similar to that proposed at the tissue level by Claes and Heigele. Chondrocytes near the reserve/proliferative zone border are subjected to combinations of high compressive hydrostatic stresses (−0.4 MPa), and cell height and width strains of −12 to +9 %, respectively, that maintain cartilage and keep chondrocytes from differentiating, whereas chondrocytes closer to the hypertrophic/calcified zone undergo combinations of lower compressive hydrostatic stress (−0.18 MPa) and cell height and width strains as low as −4 to +4 %, respectively, that promote cell differentiation toward osteogenesis; cells near the outer periphery of the growth plate structure experience a combination of low compressive hydrostatic stress (0 to −0.15 MPa) and high maximum principal strain (20–29 %) that stimulate cell differentiation toward fibrocartilage or fibrous tissue. With the ability to relate macroscopic loads to chondrocytes mechanics, this model may serve as a basis for further studies to explore the relationship between chondrocyte mechanics and mechanoregulatory bone growth theories. Furthermore, understanding the mechanobiology of growth plate cartilage may aid in developing new therapeutic interventions for bone growth-related diseases such as scoliosis, and new strategies for creating the laboratory environment necessary for tissue engineering.

Conflict of interest

conflicts of interest The authors declare that they have no conflicts of interest.

References

Allen DM, Mao JJ (2004) Heterogeneous nanostructural and nanoelastic properties of pericellular and interterritorial matrices of chondrocytes by atomic force microscopy. J Struct Biol 145(3):196–204

Amini S, Veilleux D, Villemure I (2010) Tissue and cellular morphological changes in growth plate explants under compression. J Biomech 43(13):2582–2588

Appelman TP, Mizrahi J, Seliktar D (2011) A finite element model of cell-matrix interactions to study the differential effect of scaffold composition on chondrogenic response to mechanical stimulation. J Biomech Eng 133(4):041010

Armstrong CG, Lai WM, Mow VC (1984) An analysis of the unconfined compression of articular cartilage. J Biomech Eng 106(2):165–173

Ateshian GA, Lai WM, Zhu WB, Mow VC (1994) An asymptotic solution for the contact of two biphasic cartilage layers. J Biomech 27(11):1347–1360

Bergmann G, Bender A, Graichen F, Dymke J, Rohlmann A, Trepczynski A, Heller MO, Kutzner I (2014) Standardized loads acting in knee implants. PLoS One 9(1):e86035

Bleuel J, Zaucke F, Brüggemann GP, Niehoff A (2015) Effects of cyclic tensile strain on chondrocyte metabolism: a systematic review. PloS One 10(3):e0119816

Bonnel F, Peruchon E, Baldet P, Dimeglio A, Rabischong P (1983) Effects of compression on growth plates in the rabbit. Acta Orthop Scand 54:730–733

Brown TD, Singerman RJ (1986) Experimental determination of the linear biphasic constitutive coefficients of human fetal proximal femoral chondroepiphysis. J Biomech 19(8):597–605

Burridge K, Fath K, Kelly T, Nuckolls G, Turner C (1988) Focal adhesions: transmembrane junctions between the extracellular-matrix and the cytoskeleton. Ann Rev Cell Biol 4:487–525

Bylski-Austrow DI, Wall EJ, Rupert MP, Roy DR, Crawford AH (2001) Growth plate forces in the adolescent human knee: a radiographic and mechanical study of epiphyseal staples. J Pediatr Orthop 21:817–823

Carter DR, Wong M (1988a) The role of mechanical loading histories in the development of diarthrodial joints. J Orthop Res 6(6):804–816

Carter DR, Wong M (1988b) Mechanical stresses and endochondral ossification in the chondroepiphysis. J Orthop Res 6:148–154

Carter DR, Wong M (1990) Mechanical stresses in joint morphogenesis and maintenance. In: Mow VC, Ratcliffe A, Woo SL-Y (eds) Biomechanics of diarthrodial joints, vol 2. Springer, New York, pp 155–174

Carter DR, Orr TE (1992) Skeletal development and bone functional adaptation. J Bone Miner Res 7:389–395

Carter DR, Beaupré GS (1999) Linear elastic and poroelastic models of cartilage can produce comparable stress results: a comment on Tanck et al. (J Biomech 32: 153-161, 1999). J Biomech 32(11):1255-7

Carter DR, Wong M (2003) Modelling cartilage mechanobiology. Philos Trans R Soc Lond Ser B-Biol Sci 358(1437):1461–1471

Carter DR, Orr TE, Fyhrie DP, Schurman DJ (1987) Influences of mechanical stress on prenatal and postnatal skeletal development. Clin Orthop Relat Res 219:237–250

Carter DG, Blenman PR, Beaupré GS (1988) Correlations between mechanical stress history and tissue differentiation in initial fracture healing. J Orthop Res 6:736–748

Carter DR, Beaupré GS, Giori NJ, Helms JA (1998) Mechanobiology of skeletal regeneration. Clin Orthop Relat Res 355:S41–S55

Chahine NO, Hung CT, Ateshian GA (2007) In-situ measurements of chondrocyte deformation under transient loading. Eur Cells Mater 13:100–111

Chan DD, Cai L, Butz KD, Trippel SB, Nauman EA, Neu CP (2016) In vivo articular cartilage deformation: noninvasive quantification of intratissue strain during joint contact in the human knee. Sci Rep 6:19220. doi:10.1038/srep19220

Claes LE, Heigele CA (1999) Magnitudes of local stress and strain along bony surfaces predict the course and type of fracture healing. J Biomech 32(3):255–266

Darling EM, Topel M, Zauscher S, Vail TP, Guilak F (2008) Viscoelastic properties of human mesenchymally-derived stem cells and primary osteoblasts, chondrocytes, and adipocytes. J Biomech 41(2):454–464

Farnum CE, Wilsman NJ (2011) Orientation of primary cilia of articular chondrocytes in three-dimensional space. Anat Rec 294(3):533–549

Ferguson C, Alpern E, Miclau T, Helms JA (1999) Does adult fracture repair recapitulate embryonic skeletal formation? Mech Dev 87(1):57–66

Frost HM (1990) Skeletal structural adaptations to mechanical usage (SATMU): 3—the hyaline cartilage modeling problem. Anat Rec 226(4):423–432

Frost HM (1997) Defining osteopenias and osteoporoses: another view (with insights from a new paradigm). Bone 20(5):385–391

Gao J, Williams JL, Roan E (2014) On the state of stress in the growth plate under physiologic compressive loading. Open J Biophys 4(1):13–21. doi:10.4236/ojbiphy.2014.41003

Gao J, Roan E, Williams JL (2015) Regional variations in growth plate chondrocyte deformation as predicted by three-dimensional multi-scale simulations. PLoS ONE 10(4):e0124862. doi:10.1371/journal.pone.0124862

Guilak F, Mow VC (2000) The mechanical environment of the chondrocyte: a biphasic finite element model of cell–matrix interactions in articular cartilage. J Biomech 33(12):1663–1673

Haycraft CJ, Serra R (2008) Cilia involvement in patterning and maintenance of the skeleton. Curr Top Dev Biol 85:303–332

Hert J (1976) Growth of the epiphyseal plate in circumference. Acta Anat 82:420–436

Higginson GR, Litchfield MR, Snaith J (1976) Load-displacement-time characteristics of articular cartilage. Int J Mech Sci 18(9):481–486

Hosseini A, Van de Velde SK, Kozanek M, Gill TJ, Grodzinsky AJ, Rubash HE, Li G (2010) In-vivo time-dependent articular cartilage contact behavior of the tibiofemoral joint. Osteoarthr Cartil 18(7):909–916

Hueter C (1863) Anatomische Studien an den Extremitätengelenken Neugeborener und Erwachsener. Virchows Archiv 26(5):484–519

Jensen CG, Poole CA, McGlashan SR, Marko M, Issa ZI, Vujcich KV, Bowser SS (2004) Ultrastructural, tomographic and confocal imaging of the chondrocyte primary cilium in situ. Cell Biol Int 28(2):101–110

Katta J, Jin Z, Ingham E, Fisher J (2009) Effect of nominal stress on the long term friction, deformation and wear of native and glycosaminoglycan deficient articular cartilage. Osteoarthr Cartil 17(5):662–668

Kronenberg HM (2003) Developmental regulation of the growth plate. Nature 423(6937):332–336

Lai VK, Hadi MF, Tranquillo RT, Barocas VH (2013) A multiscale approach to modeling the passive mechanical contribution of cells in tissues. J Biomech Eng 135(7):071007

Leipzig ND, Athanasiou KA (2005) Unconfined creep compression of chondrocytes. J Biomech 38(1):77–85

Lerner AL, Kuhn JL (1997) Characterization of regional and age-related variations in the growth of the rabbit distal femur. J Orthop Res 15(3):353–361

Lerner AL, Kuhn JL, Hollister SJ (1998) Are regional variations in bone growth related to mechanical stress and strain parameters? J Biomech 31(4):327–335

Loboa EG, Wren TAL, Beaupré GS, Carter DR (2003) Mechanobiology of soft skeletal tissue differentiation: a computational approach of a fiber-reinforced poroelastic model based on homogeneous and isotropic simplifications. Biomech Model Mechanobiol 2(2):83–96

Mackie EJ, Ahmed YA, Tatarczuch L, Chen KS, Mirams M (2008) Endochondral ossification: how cartilage is converted into bone in the developing skeleton. Int J Biochem Cell Biol 40(1):46–62

Mann RA, Hagy J (1980) Biomechanics of walking, running, and sprinting. Am J Sports Med 8(5):345–350

Mao JJ, Nah HD (2004) Growth and development: hereditary and mechanical modulations. Am J Orthod Dentofac Orthop 125(6):676–689

Ng L, Hung H-H, Sprunt A, Chubinskaya S, Ortiz C, Grodzinsky A (2007) Nanomechanical properties of individual chondrocytes and their developing growth factor-stimulated pericellular matrix. J Biomech 40(5):1011–1023

Pauwels F (1960) Eine neue Theorie über den Einfluß mechanischer Reize auf die Differenzierung der Stützgewebe. Z Anat Entwicklung 121(6):478–515

Pauwels F (1965) Grundriβ einer Biomechanik der Frakturheilung: Gesammelte Abhandlungen zur funktionellen Anatomie des Bewegungsapparates. Springer, Berlin

Pauwels F (1980) Biomechanics of the locomotor apparatus. Springer, New York

Piszczatowski S (2011) Material aspects of growth plate modelling using Carter's and tokes's approaches. Acta Bioeng Biomech 13(3):3–14

Radhakrishnan P, Lewis NT, Mao JJ (2004) Zone-specific micromechanical properties of the extracellular matrices of growth plate cartilage. Ann Biomed Eng 32(2):284–291

Sachs F (1991) Mechanical transduction by membrane ion channels: a mini review. Mol Cell Biochem 104(1–2):57–60

Safran MR, Eckardt JJ, Kabo JM, Oppenheim WL (1992) Continued growth of the proximal part of the tibia after prosthetic reconstruction of the skeletally immature knee: estimation of the minimum growth force in vivo in humans. J Bone Joint Surg Am 74(8):1172–1179

Seeger-Nukpezah T, Golemis EA (2012) The extracellular matrix and ciliary signaling. Curr Opin Cell Biol 24(5):652–661

Shao YY, Wang L, Welter JF, Ballock RT (2012) Primary cilia modulate Ihh signal transduction in response to hydrostatic loading of growth plate chondrocytes. Bone 50(1):79–84

Shapiro F, Holtrop ME, Glimcher MJ (1977) Organization and cellular biology of the perichondrial ossification groove of Ranvier. J Bone Joint Surg 59–A:703–723

Solomon L (1966) Diametric growth of the epiphysial plate. J Bone Joint Surg Br 48(1):170–177

Stokes IAF (2002) Mechanical effects on skeletal growth. J Musculoskelet Neuronal Interact 2(3):277–280

Stokes IAF, Clarck KC, Farnum CE, Aronsson DD (2007) Alterations in the growth plate associated with growth modulation by sustained compression or distraction. Bone 41:197–205

Stokes IAF, Aronsson DD, Dimock AN, Cortright V, Beck S (2006) Endochondral growth in growth plates of three species at two anatomical locations modulated by mechanical compression and tension. J Orthop Res 24:1327–1334

Temiyasathit S, Jacobs CR (2010) Osteocyte primary cilium and its role in bone mechanotransduction. Ann N Y Acad Sci 1192(1):422–428

Tutorino JC, Khubchandani ZG, Williams JL, Cobb CM, Schmidt TL (2001) Can the epiphyseal growth plate be injured in compression?. In: Transactions of the 47th annual meeting of the orthopaedic research society, vol 26, p 353

Valteau B, Grimard G, Londono I, Moldovan F, Villemure I (2011) In vivo dynamic bone growth modulation is less detrimental but as effective as static growth modulation. Bone 30;49(5):996–1004

Villemure I, Stokes IAF (2009) Growth plate mechanics and mechanobiology: a survey of present understanding. J Biomech 42(12):1793–1803

Vinardell T, Rolfe RA, Buckley CT, Meyer EG, Ahearne M, Murphy P, Kelly DJ (2012) Hydrostatic pressure acts to stabilise a chondrogenic phenotype in porcine joint tissue derived stem cells. Eur Cells Mater 23:121–134

Volkmann R (1862) Verletzungen und Krankenheiten der Bewegungsorgane. In: von Pitha FR, Billroth T (eds) Handbuch der allgemeinen und speciellen Chirurgie Bd II Teil II. Ferdinand Enke, Stuttgart

Watson PA (1991) Function follows form: feneration of intracellular signal by cell-deformation. FASEB J 5(7):2013–2019

Winyard P, Jenkins D (2011) Putative roles of cilia in polycystic kidney disease. Biochim Biophys Acta (BBA)-Mol Basis Dis 1812(10):1256–1262

Wong M, Carter DR (1990) A theoretical model of endochondral ossification and bone architectural construction in long bone ontogeny. Anat Embryol 181:523–532

Wong M, Siegrist M, Goodwin K (2003) Cyclic tensile strain and cyclic hydrostatic pressure differentially regulate expression of hypertrophic markers in primary chondrocytes. Bone 33(4):685–693

Wosu R, Sergerie K, Lévesque M, Villemure I (2012) Mechanical properties of the porcine growth plate vary with developmental stage. Biomech Model Mechanobiol 1;11(3–4):303–312